NEURORADIOLOGY

REVIEW

Neuro-otologic applications of MRI

Nail Bulakbaşı, Yüksel Pabuşçu

ABSTRACT
Magnetic resonance imaging (MRI) has increasingly new applications in neuro-otology. The aim of this review was to summarize MRI applications in neuro-otology and make a correlation between neuro-otologic anatomy and MR images. Different MRI techniques have been described in the imaging of different neuro-otologic structures. In particular, we discuss the effectiveness, indications, and techniques of MRI in the demonstration of neuro-otologic tracts and their related pathologies. MRI should be the first choice imaging modality for the evaluation of retro-cochlear pathologies.

Key words: • neuro-otology • magnetic resonance imaging

Computed tomography (CT) has been the basic technique for evaluating the temporal bone since its establishment in the early 1970s. Isotropic fine sections with a bone algorithm obtained in different axes, and their 3D reconstruction are the most effective methods for visualizing the anatomy of the bone labyrinth and for evaluating any pathological changes to the bone component, such as in trauma, structural or developmental defects, and metabolic diseases (1, 2). Thus, CT remains the primary modality for temporal bone imaging; however, CT is not capable of displaying the membranous labyrinth and the nerve pathways leaving it (1, 2). The 3 most common reasons for otoradiological examinations, excluding trauma, are vertigo, tinnitus, and sudden loss of hearing, which are the result of pathologies arising mostly from the membranous labyrinth, nerve pathways, or from anatomic structures related to them. Magnetic resonance imaging (MRI) is the most effective technique for the evaluation of these structures and their pathologies (3–13). Using MRI, temporal and cisternal portions of the 7th and 8th cranial nerves and their nuclei in the brain stem, the ascending, descending, and connecting pathways, and primary-secondary hearing center pathologies, as well as lesions related to these structures can be displayed (4, 5, 9–11, 13). Despite the latest advances in imaging technology, evaluating the anatomical changes in hearing and balance organs, and the nerve pathways leaving them remains a difficult procedure that must be performed by an experienced specialist. This review aimed to discuss the effectiveness of MRI in imaging neuro-otologic anatomical structures and changes within them, and to explain the techniques used for diagnosing neuro-otologic lesions by presenting appropriate examples.

Technique

A standard head coil is used for neuro-otologic MRI examinations. Superficial coils that display the temporal bone in detail can also be used, but in order to also include the brain stem and brain it is necessary to switch to a standard head coil. Currently, multichannel coils that enable parallel imaging are used for this purpose. Thin section (2–3 mm) continuous T1-weighted (T1W) and T2-weighted (T2W) sections of the posterior fossa are taken for basic examinations in at least 2 planes (preferably transverse and coronal). To display brain and brain stem lesions, FLAIR and T1W images must be focused on the brain. High resolution, thin section, fat suppressed, fast spin-echo, or 3D fast gradient-echo T1W sections must be obtained to differentiate inflammation and tumoral lesions following intravenous paramagnetic contrast agent injection. A standard temporal bone examination is finalized with 3D high-resolution heavily T2W MR cisternography sequences (e.g., CISS, FASE, FIESTA, balanced FFE), with visualization of the inner ear structures and

From the Department of Radiology (N.B. ✉ *nbulak@gata.edu.tr*), Gülhane Military Medical Academy, Ankara, Turkey; and the Department of Radiology (Y.P.), Celal Bayar University School of Medicine, Manisa, Turkey.
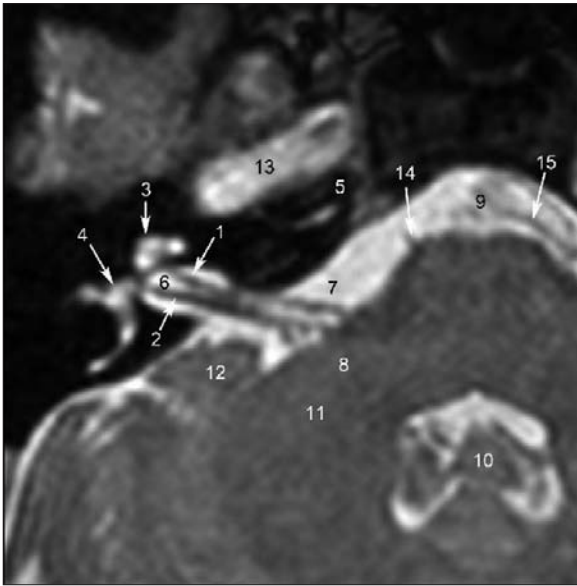
Figure 1. Transverse 3D gradient echo T2-weighted thin section MR image of the internal acoustic canal and pontocerebellar angle cistern. (1) Cochlear nerve; (2) vestibular nerve; (3) cochlea; (4) vestibule; (5) petrous apex; (6) fundus of the internal acoustic canal; (7) pontocerebellar angle cistern; (8) vestibulocochlear nuclei; (9) prepontine cistern; (10) fourth ventricle; (11) middle cerebellar pedicle; (12) flocculus; (13) petrous segment of the internal carotid artery; (14) nervus abducens; (15) anterior inferior cerebellar artery.
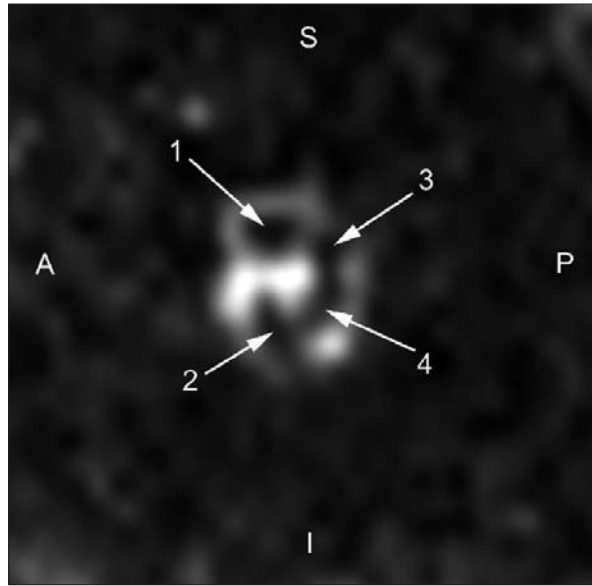
Figure 2. Oblique-sagittal 3D gradient echo T2-weighted thin section MR image taken perpendicular to the internal acoustic canal. Structures can be identified as follows: Facial nerve (1) is present at the anterior superior quadrant; cochlear nerve (2) at the anterior inferior quadrant; superior (3) and inferior (4) branches of the vestibular nerve at the posterior superior and inferior quadrants, respectively.
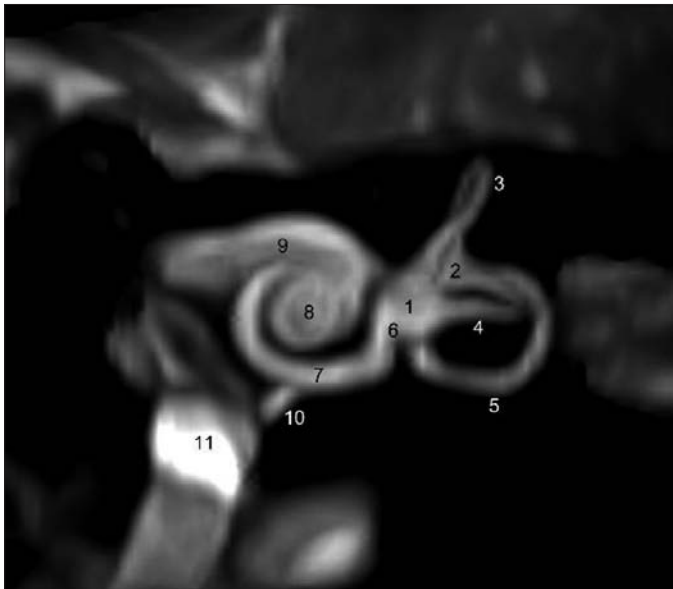
Figure 3. MR image of the membranous labyrinth obtained using a 3D maximum intensity projection (MIP) algorithm. (1) Vestibule; (2) common crus; (3) superior semicircular canal; (4) lateral semicircular canal; (5) posterior semicircular canal; (6) ductus reuniens (7) basal turn of the cochlea; (8) cochlea; (9) cochlear nerve; (10) endolymphatic canal; (11) jugular bulb.

ing centers and the pathways leaving it, are also helpful (15). With the aid of different software methods, like multi-plane reformation, which is applied to 3D thin section images, volume rendering, maximum intensity projection (MIP), tissue segmentation, and virtual endoscopy, detailed visualization can be made of the neuronal components of the ear.

Examination can be finalized in routine practice by obtaining axial and coronal thin section T1W and T2W sequences, as well as a heavily T2W MR cisternography sequence and T1W sections using contrast material; as obtaining the above defined sequences take a long time.

Anatomy

Neuro-otologic structures that can be basically evaluated with MRI include the following: the membranous labyrinth, the ascending and descending connection pathways of hearing and balance, cranial nerves, and the primary-secondary centers of hearing and balance (Figs. 1, 2) (16–20).

The cochlea, vestibule, semicircular channels (SCCs), and endolymphatic canal can be seen with MRI, whereas vestibular components (sacculus, utriculus, and round window) are not vis-

neuronal pathways (14). MR angiography must be added to the examination to evaluate vascular pathologies or pulsatile tinnitus (2). When retrocochlear pathology is detected, diffusion and/or perfusion MR imaging and advanced

techniques that help to differentiate normal tissues from lesions, like MR spectroscopy, can be used. Diffusion tensor imaging and cortical activation, to display the relationship between a lesion and the primary-secondary hear-

Figure 4. Schematic view superimposed on coronal MR image of the ascending hearing pathways. (1) Membranous labyrinth; (2) 8th cranial nerve; (3) inferior olivary nucleus; (4) trapezoid body; (5) superior olivary nucleus; (6) anteroventral cochlear nucleus; (7) posterolateral cochlear nucleus; (8) dorsal cochlear nucleus; (9) lateral lemniscus; (10) lateral lemniscus nucleus; (11) inferior colliculus; (12) medial geniculate nucleus; (13) superior temporal gyrus (A1 and A2 motor centers of hearing).
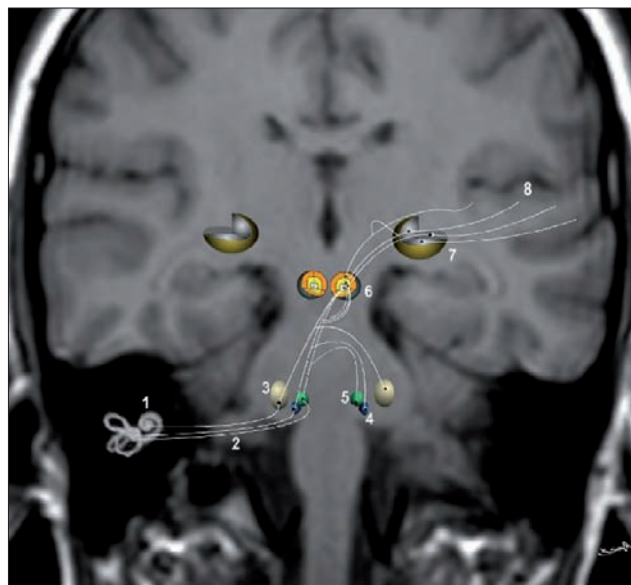
Figure 5. Schematic view superimposed on coronal MR image of the descending hearing pathways. (1) Membranous labyrinth; (2) 8th cranial nerve; (3) dorsal cochlear nucleus; (4) inferior olivary nucleus; (5) superior olivary nucleus; (6) inferior colliculus; (7) medial geniculate nucleus; (8) superior temporal gyrus (A1 and A2 motor centers of hearing).

ible (Fig. 3). The cochlear canal is a spiral structure that includes 3 potential cavities in which endolymph and perilymph circulate. It connects to the sacculus via the ductus reuniens at the base of the spiral. The vestibule is the structure that connects the SCCs to the cochlea; it senses and plays a role in adaptation to static balance and air pressure changes. The posterior, superior, and lateral SCCs have a diameter of 1 mm, make a turn of 2/3 of a circle, and end with an expansion at their front edges, called the ampulla. The non-expanding superior and posterior crura merge and make the common crus. Three SCCs drain into the vestibule via 5 openings. The saccular canal, which originates from the sacculus, and the utricular canal, which originates from the utriculus, merge and create the endolymphatic canal sinus, which regulates endolymphatic pressure. The endolymphatic canal, which is located in the vestibular aqueduct, ends with the endolymphatic sac at the dura covering the petrous bone. The width of the endolymphatic canal is 0.1–0.2 mm in the isthmus and 0.5 mm in the middle part in adults.

Nerve pathways for hearing and balance, cruise quite differently and complicated. The hearing pathways are divided into 2 basic groups: ascending (Fig. 4) and descending (Fig. 5). Primary fibers originating from the cochlea travel through the cochlear branch of the 8th cranial nerve and terminate in the dorsal, posterolateral, and anteroventral cochlear nucleus complex located in the restiform body in the pontomedullary junction. Fibers originating from that location are distributed in a very complex manner; fibers originating from the posterolateral and anteroventral cochlear nuclei terminate at the ipsilateral lateral superior olivary nucleus, whereas a group of fibers originating from the anteroventral cochlear nucleus terminate in the contralateral superior olivary nucleus, passing via the medial lemniscus and medial nucleus of the trapezoid body. The superior olivary nucleus is the first nucleus in which fibers coming from both ears merge in the brain stem. A group of fibers originating from the ipsilateral, posterolateral, and anteroventral cochlear nuclei, and the superior olivary nucleus progress to the contralateral inferior colliculus and lateral lemniscus nucleus via the lateral lemniscus. The majority of fibers originating from the ipsilateral superior olivary nucleus reach the medial geniculate nucleus via the ipsilateral inferior col-

liculus. Primary afferent fibers originating from the anterior segment of the medial geniculate nucleus terminate in the primary hearing center (A1) located in the superior temporal gyrus at the inferior surface of the Heschl gyrus and lateral sulcus, whereas fibers originating from the inner segment terminate in the secondary hearing center (A2) located in the posterior transverse gyrus. Reciprocal fibers are present between A1 and A2, and between the 2 opposite centers. Around A1, behind the superior temporal gyrus, the common hearing center is located and is connected to A1 with the arcuate fascicle. The common center is connected to the Wernicke zone at the level of the supramarginal gyri and to Broca zone at the level of the pars triangularis.

The descending pathways of hearing maintain a feedback loop between the upper and lower centers (Fig. 5). Descending fibers originating from the hearing cortex go to the ipsilateral medial geniculate nucleus and outer nucleus of the inferior colliculus, which regulates the relationship between A1 and A2, and the common centers. While fibers originating from the central nucleus of the inferior colliculus progress to the ipsilateral and contralateral superior olivary and dor-
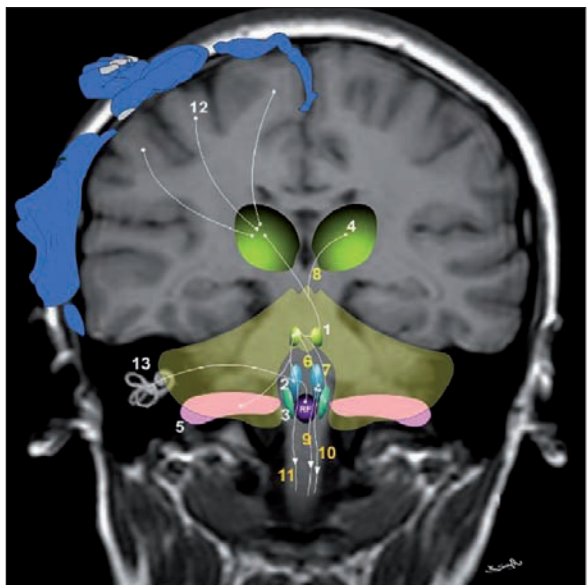
Figure 6. Schematic view superimposed on coronal MR image of the vestibular sensorial pathways. (1) Fastigial nucleus; (2) vestibular nucleus; (3) accessory olivary nucleus; (4) hypothalamus; (5) flocculonodular nodule; (6) fastigo-vestibular pathway; (7) fastigo-olivary pathway; (8) fastigo-thalamic pathway; (9) medial vestibulospinal pathway; (10) lateral vestibulospinal pathway; (11) fastigo-spinal pathway; (12) motor cortex connections; (13) vestibular apparatus; reticular formation (RF).

sal nuclei, those originating from the pericentral nucleus go to the ipsilateral and contralateral superior olivary nuclei. Fibers originating from the superior olivary nucleus in the olivocochlear bundle travel in the vestibular branch of the 8th cranial nerve. Lateral olivocochlear fibers terminate in the ipsilateral inner hairy cells, whereas medial fibers terminate in the ipsilateral and contralateral outer hairy cells.

The vestibular pathways (Fig. 6) begin with a synapse formation between the projections of type 1–2 hairy cells, which are located in the vestibule and SCCs, and in the soma of primary sensory fibers that are located in the vestibular ganglions. Primary sensory fibers responsible for the proprioceptive senses, which are sensitive to head movement, are carried in the vestibular nerve and terminate in the vestibular nucleus complex located at the base of the fourth ventricle. This complex consists of the superior, lateral, medial, and inferior vestibular nuclei. Fibers originating from the medial and lateral vestibular nuclei travel along the medial and lateral vestibulospinal pathways inside the spinal cord and regulate extensor muscle tonus; thus, maintaining the upright position of the body in opposition to gravity. Fibers originating from the medial and inferior vestibular nucleus are carried along the vestibulocerebellar pathway bilaterally and they connect to the cerebellum to maintain balance while walking. Upper fibers originating from all the nuclei travel up in the longitudinal fascicle and connect to the 3rd, 4th, and 6th cranial nerves, and thalamus, maintaining adaptation to darkness and the tonus of the extraocular muscles in order to fix the eyeballs to a constant point.

Pathology
Vascular lesions

Congenital vascular anomalies of the temporal bone are as follows: absence and hypoplasia of the internal carotid artery, and aberrant or high localization of the jugular bulb. All of these vascular anomalies can be visualized with MR angiography and 3D T2W reformatted images (2). In particular, in the absence of the internal carotid artery, changes appear in cerebral circulation and areas at risk can be exposed using MR angiography and perfusion MRI (Fig. 7)

Apart from vascular anomalies, the most common causes of sudden hearing loss, tinnitus, and especially vertigo are arteriovenous malformations located in the brain stem, cavernous angiomas, developmental venous anomalies, ischemia and infarct of the brain stem, and aneurysm, dolichoectasia, or

vascular rings located in the pontocerebellar angle cistern.

Classical views and enhancement properties of T1W and T2W MRI sequences are sufficient for the diagnosis of developmental venous anomalies, cavernous angiomas, and arteriovenous malformations (Fig. 8); however, for the diagnosis of vertebrobasilar dolichoectasia (>4.5 mm), aneurysm, and vascular rings, 3D T2W reformatted images are needed in addition to MR angiography (21). These vascular lesions, which can cause vertigo, hemifacial spasm, and trigeminal or facial neuralgia, may extend inside the pontocerebellar angle cistern, compress the 7th and 8th cranial nerves, and cause displacement (Fig. 9). Moreover, tumoral structures, such as ependymomas, or leptomeningeal structures after chronic capillary or venous bleeding, subpial tissue, and superficial siderosis caused by intracellular or extracellular hemosiderin accumulation in the spinal cord and cranial cells are seen as signal-free superficial regions.

Lacunar or diffuse brain stem infarcts caused by occlusion of the pontine perforators, especially in elderly and hypertensive cases, can be visualized using diffusion and/or perfusion imaging within the first 6 h. Significant diffusion restriction on diffusion weighted MR images (Fig.10), and decreased perfusion (relative cerebral blood flow) can be seen (22). There is the potential to reduce both infarct size and the severity of clinical impairment when imaging is performed in a timely fashion and various procedures for vessel recanalization are undertaken. Therefore, cochlear artery emboli and subsequent end-organ ischemia, one of the rare causes of sudden unilateral hearing loss in elderly patients, cannot be seen using current MRI techniques.

By the way, labyrinthine and cochlear hemorrhages caused by coagulopathies, tumors, operations, or labyrinthitis can only be seen with MRI (4). In addition, imaging of blood products in different stages and loss of endolymph signal can be seen with MRI, both of which appear hyperintense after posthemorrhagic fibrosis in T2W gradient echo sequences (23).

Congenital anomalies

CT is still the most superior tool for imaging inner ear anomalies that affect the bony and membranous labyrinths.
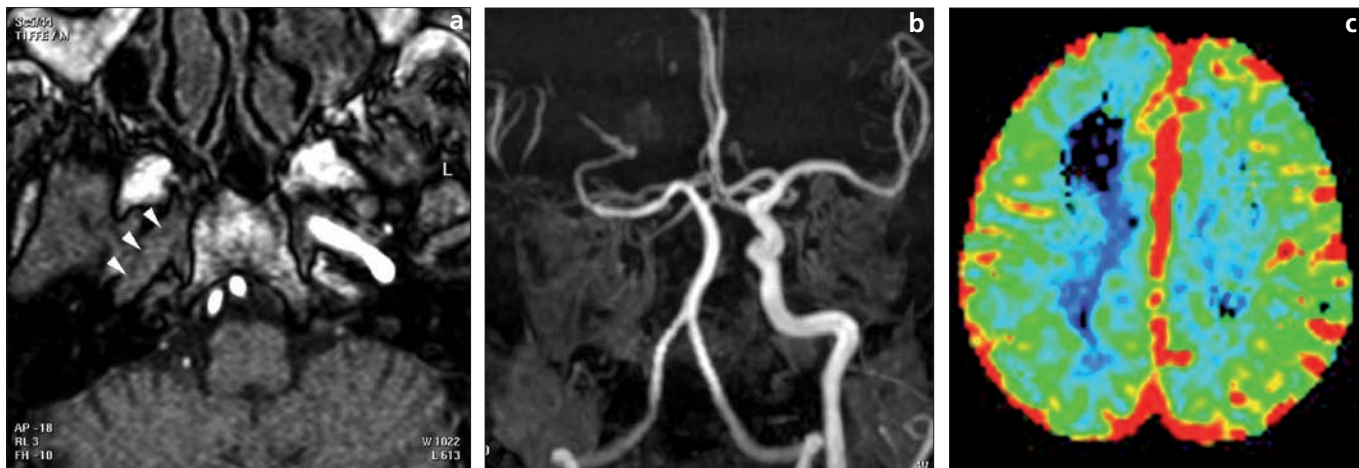
Figure 7. a–c. Aplasia of the internal carotid artery. On transverse T1-weighted MR image **(a)**, the right carotid canal does not appear to have developed normally *(arrowheads)* because the aplastic carotid segment and its cavity were obliterated by bone tissue. On coronal cerebral MR angiography **(b)**, flow in the right internal carotid artery cannot be seen, whereas the right middle and anterior cerebral arteries are fed from the left internal carotid artery. Transverse perfusion MRI (rCBF map) **(c)** of the patient shows reduced perfusion in the right cerebral hemisphere in comparison to the left.
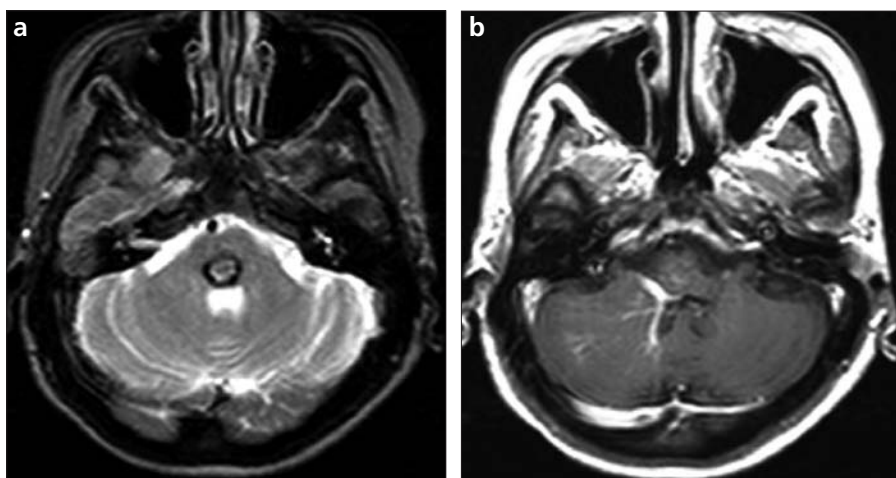
Figure 8. a, b. Vascular malformations. On axial T2-weighted MR image **(a)**, a typical heterogeneous-hyperintense cavernous hemangioma is evident, with signal-void halo due to chronic hemorrhagic products at the posterior section of the pons. A subsequent contrast enhanced T1-weighted MR slice **(b)** of the same patient shows accompanying congenital venous anomaly and related caput medusae-shaped distribution. The coexistence of these 2 vascular malformations is called mixed vascular malformation.
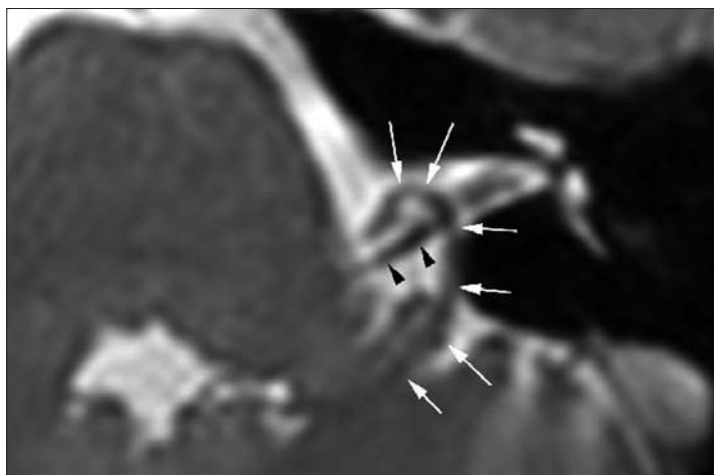
Figure 9. Vascular ring. On transverse T2-weighted MR image, a vascular ring formation of the left anterior inferior cerebellar artery *(white arrows)* near the left 8th nerve *(black arrowheads)* is seen.

Even though congenital anomalies, such as the absence of the cupula or the presence of a common cavity, can be seen with MRI, it does not provide additional advantages over CT. Nevertheless, for some particular subjects, like visualization of cochlear circulation, exhibition of scalar space symmetry, and evaluation of the modiolus and the posterior membranous labyrinth, fine section T2W MRI sequences are more informative than CT (24).

Cochlear implantation is the most effective method of treatment for congenital bilateral moderate (>90 dB) and severe (70–90 dB) hearing loss in patients >2 years of age that have not benefitted from external hearing devices and who are eager for complete rehabilitation (25). In such cases both CT and MRI must be included in the preoperative radiological evaluation to aid in the following: deciding into which side the device is going to be implanted, determining the integrity of the cochlea, consideration of the round window niche approach, measuring the degree of mastoid ventilation, and, most importantly, the evaluation of contraindications for implantation surgery (24). Contraindications include: mastoid cell ventilation insufficiency; a hypoplastic mastoid bone; congenital cholesteatoma or inflammation of mastoid cells, which fail to reach the facial nerve recess during surgery; abnormal location of the facial nerve, internal carotid artery, or sigmoid sinus; a narrow internal acoustic canal (<2 mm); absence of the modio-
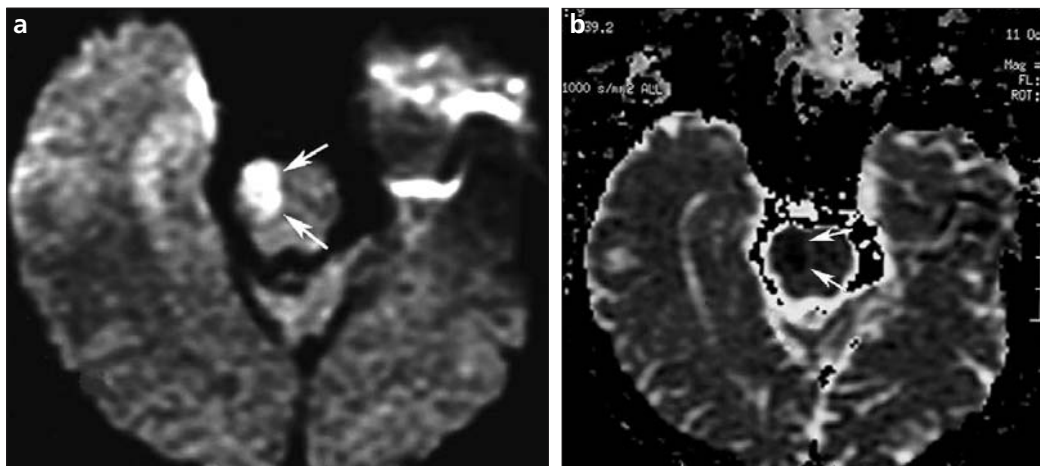
Figure 10. a, b. Acute ischemia of the brain stem. Diffusion restriction displayed as hyperintensity on axial diffusion weighted MR image **(a)** and hypointensity on ADC map image **(b)** at the right half of the pons, typical finding of acute arterial ischemia.
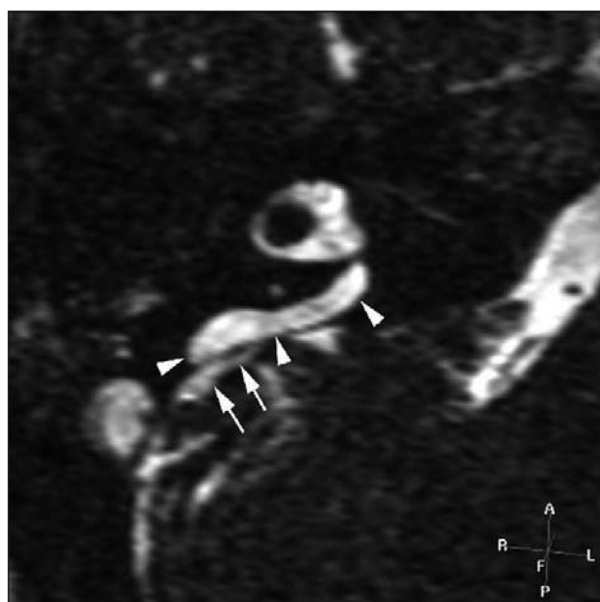
Figure 11. Endolymphatic hydrops. 3D gradient echo T2-weighted transverse MR image shows swollen endolymphatic canal *(arrowheads)* ending in a swollen endolymphatic sac *(arrows).*

lus; absence or hypoplasia of the cochlear nerve (<0.4 mm, or thinner than facial nerve); membranous labyrinth malformations; Gusher ear; absence of the round window or niche, or stenosis of either of them secondary to Paget's disease; osteosclerosis; Lobstein disease; post-meningitis labyrinthitis; cochlear ossification or fibrosis that impairs and/or reduces circulation of endolymph or perilymph (24). MRI is more reliable than CT in detecting the aperture of the scala tympani, presence of the cochlear nerve, visualization of cochlear sclerosis or fibrosis, and determining pathologies affecting the sensory and motor pathways of hearing (14, 24, 26).

Using 3D T2W gradient echo MRI sequences, swollen endolymphatic areas can be visualized in cases of endolymphatic hydrops, which is associated with episodic vertigo, vomiting, and hearing loss (Fig. 11). Detection of the endolymphatic sac and opacity in both the cochlea and vestibule on T1W images support the diagnosis (2, 27).

Infectious and inflammatory diseases

Infection and inflammation of the temporal bone are the 2 most common otologic pathologies. They usually originate from otologic sources and can be evaluated effectively using high resolution CT. Inflammatory and infectious pathologies that cause neuro-otologic

symptoms by affecting inner ear structures and the internal acoustic canal are cholesteatoma, petrous apicitis, cholesterol granuloma, and mucocele, in which MRI can be beneficial. Cholesterol granulomas are seen as hyperintense in T1W and T2W sequences and do not enhance. On the contrary, petrous apicitis and mucocele may cause erosion and expansion in affected bone tissue, and are seen as hypointense on T1W and hyperintense on T2W images; they also enhance heterogeneously, especially in fat suppressed T1W sections. Cholesteatomas can be mistaken for these pathologies, and can be differentiated by detecting diffusion restriction on diffusion-weighted sequences (28). MRI plays an important role in differentiating the accompanying postoperative granulation tissue and acquired cholesteatoma. Granulation tissue typically shows enhancement in MRI, whereas cholesteatomas do not (29).

In acute labyrinthitis, enhancement may be evident in the membranous labyrinth on contrasted T1W images. Additionally, on T1W images the hemorrhagic component is hyperintense (5). An accompanying fistula is usually present. Enhancement of the membranous labyrinth can be seen in labyrinth schwannomas, apart from labyrinthitis (4). Chronic stage fibrotic tissue can best be seen on thin section T2W images (2, 4). It is important to detect the extension of these changes prior to cochlear implantation. In these cases, T1W images without contrast medium must be obtained in order to exclude intra-labyrintheal hemorrhage, which appears hyperintense.
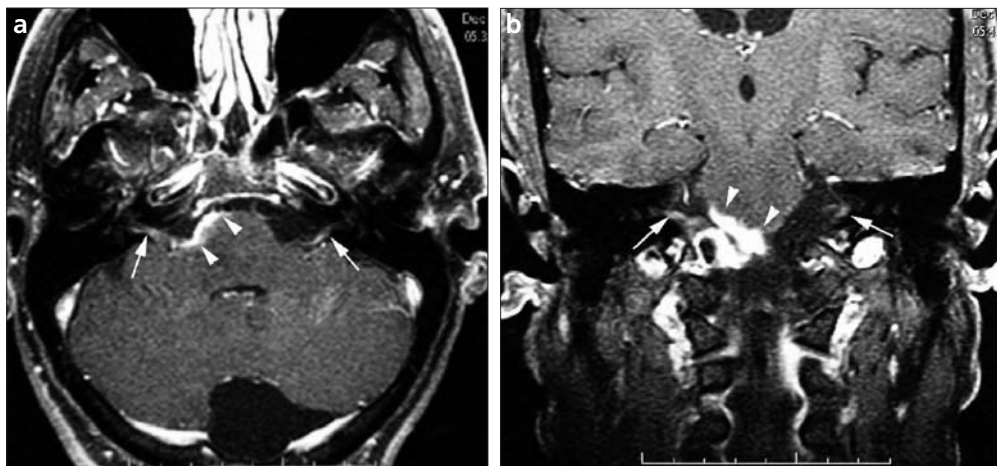
Figure 12. a, b. Basal meningitis. On contrast enhanced T1-weighted transverse **(a)** and coronal **(b)** MR sections, inflammatory thickening and enhancement of the dura covering both pontocerebellar angle cisterns *(arrowheads)*, and extension to both internal acoustic canals *(arrows)* can be seen.
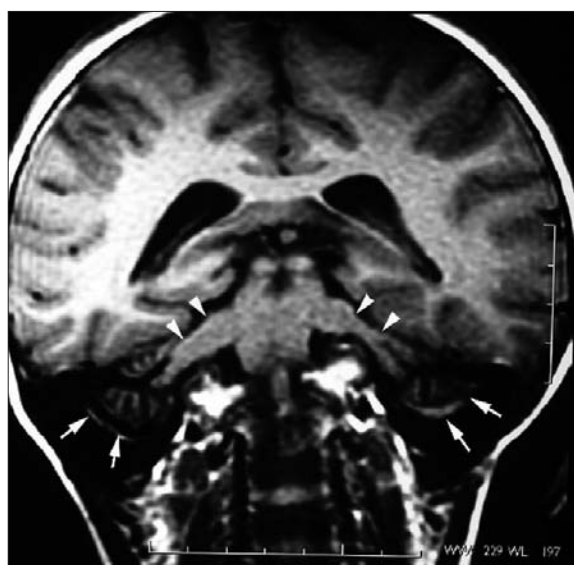
Figure 13. Osteogenesis imperfecta. Collapse of the cerebellar hemisphere through the temporal bone *(arrows)* and secondary deformation of the cerebellar pedicles *(arrowheads)* are evident on coronal T1-weighted MR image.
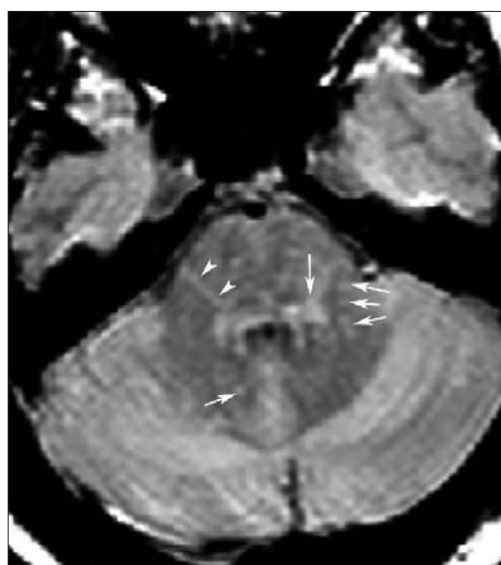
Figure 14. Multiple sclerosis. On transverse proton density MR image, involvement along all the length of right 8th nerve *(arrowheads)*, and demyelinating plaques at the cerebellum and left middle cerebellar pedicle *(arrows)* are seen.

Diffuse meningeal thickening and enhancement is evident in the pontocerebellar angle cistern and internal acoustic canal in cases of viral, bacterial, or tuberculosis meningitis (6). These are not only typical for meningitis, but can also be observed in neurosarcoidosis, meningioangiomatosis, hemangioblastomatosis, and lymphoma (Fig. 12). In its advanced stage, narrowing and obliteration of the basal cisterns (because of inflammatory fibrosis), or increased venous pressure and malabsorption of CSF due to accompanying dural sinus thrombosis results in hydrocephalus (2, 6).

Encephalocele formation due to a probable tegmen or sinus defect must be taken into consideration when a soft tissue mass is observed inside the temporal bone (30). In particular, coronal T2W and enhanced T1W series must be obtained to show an encephalocele in order to avoid fatal surgical complications.

Otodystrophies

The presence and penetration of bone dysplasia affecting the temporal bone can best be evaluated using high resolution CT; therefore, for cranial nerve paralysis in the advanced stages of polyostotic fibrous dysplasia, MRI can support the diagnosis by displaying narrowing and occlusion in bone cavities. Furthermore, in osteogenesis imperfecta, deformation in the petrous and mastoid processes of the temporal bone, and herniation or compression of cerebral tissue through these bones can be observed as a result of dislocation of the softened bones of the basis cranii due to gravity (Fig. 13) (31). In such cases, CSF flow changes at the level of the pontocerebellar angle cistern and craniocervical junction can be displayed by using phase-contrast MRI techniques.

Multiple sclerosis

Brain stem involvement in multiple sclerosis is common and may display
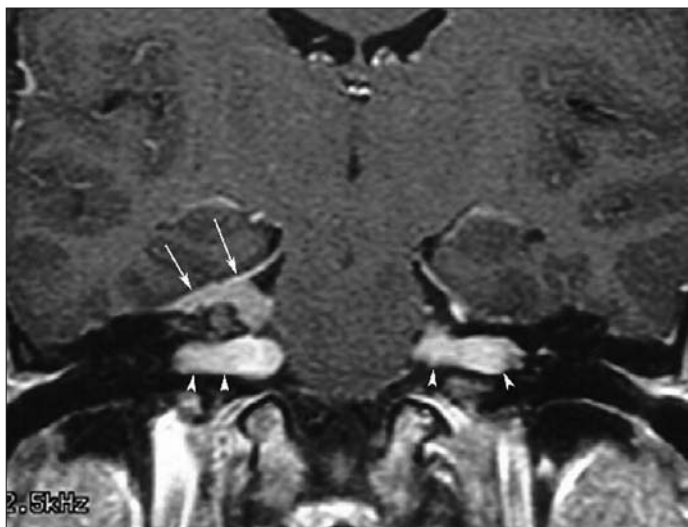
Figure 15. Neurofibromatosis, type 2 (NF2). On coronal contrast enhanced T1-weighted MR image, the coexistence of bilateral vestibular schwannomas located in both internal acoustic canals *(arrowheads)* and an en-plaque meningioma *(arrows)* at the level of tentorium are typical of NF2.
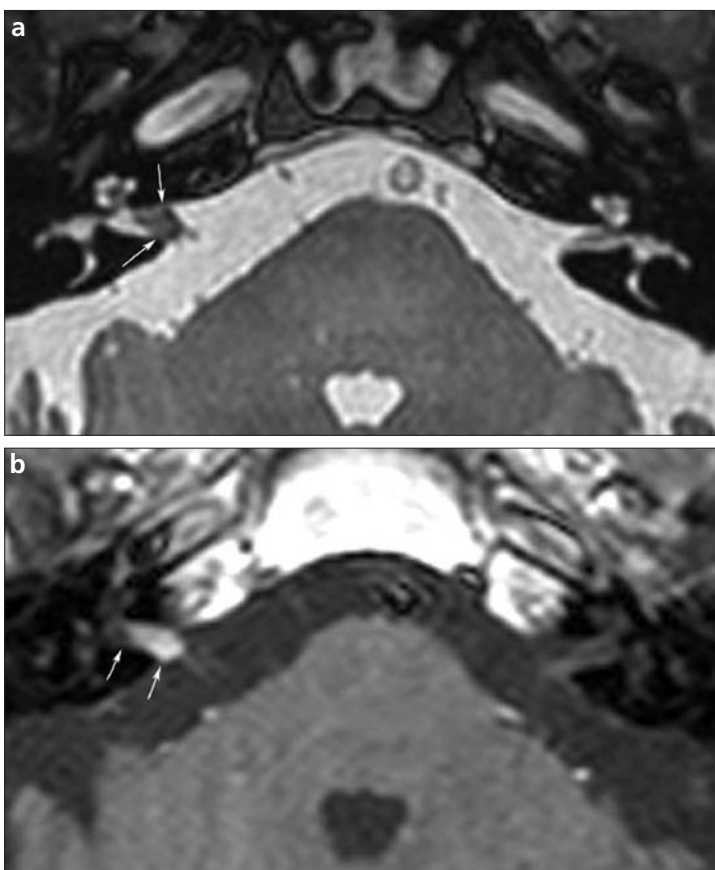
Figure 16. a, b. Vestibular schwannoma. On transverse 3D gradient echo T2-weighted **(a)** and contrast enhanced T1-weighted **(b)** MR images, a tumoral lesion *(arrows)* partially filling the right internal acoustic canal, but not affecting the fundus, cochlea, or the vestibule, is shown.

itself as loss of hearing (Fig. 14). Typical hyperintense lesions on T2W images do not enhance, except in the acute phase, and do not contain peripheral edema. On the other hand, rare involvement of the 7th and 8th cranial nerves may occur, but such involvement is too insignificant or scattered to be observed by radiological methods (32).

Tumors

Tumors, which are one of the most basic indications in neuro-otologic MRI studies, are generally divided into 2 groups with respect to the involvement of the pontocerebellar angle cistern or the brain stem, and the hearing center.

Vestibular schwannoma, meningioma, dermoid/epidermoid tumor, and arachnoid cyst are the most common tumors that occupy the pontocerebellar angle cistern, whereas facial schwannoma, other cranial nerve schwannomas, labyrinthine schwannoma, and eosinophilic granuloma should also be considered in the differential diagnosis (33, 34).

Vestibular schwannomas, which constitute 80%–90% of pontocerebellar angle tumors, present with unilateral sensorineural hearing loss and may cause tinnitus, vertigo, facial paralysis, and abnormal gait (2, 3). Typically, in type 2 neurofibromatosis, they are bilateral and appear at a young age (<21 years) (Fig. 15). Factors affecting the success of hearing-sparing surgery carried out in these cases are location and size of the tumor, enhancement of the facial nerve, tumor-nerve adhesions, tumoral involvement of the cochlear fossa and internal acoustic canal fundus, increased pressure in the internal acoustic canal, and loss of signal intensity inside the labyrinth (7, 8, 35–39). MRI is significantly superior in displaying these factors when compared to other imaging methods (2, 16). For this reason, 3D T2W and enhanced fat suppressed T1W sequences must be obtained (7). With this method, it is possible to both distinguish tumor from fat tissue around the internal acoustic canal and to determine if there is bleeding inside the tumor (Fig. 16).

Meningiomas typically appear isointense compared to gray matter on T1W and T2W series, and display intense enhancement in MRI (Fig. 17) (2, 4, 5). The hypointensity of the lesion becomes prominent as its internal fibrous component increases; therefore, the predominance of angioblastic or syncytial components results in hyperintensity on T2W images (40). Although the enlarged feeding arteries of these hypervascular tumors typically appear as signal-void tubular structures, this finding can also occasionally be seen in schwannomas (2).
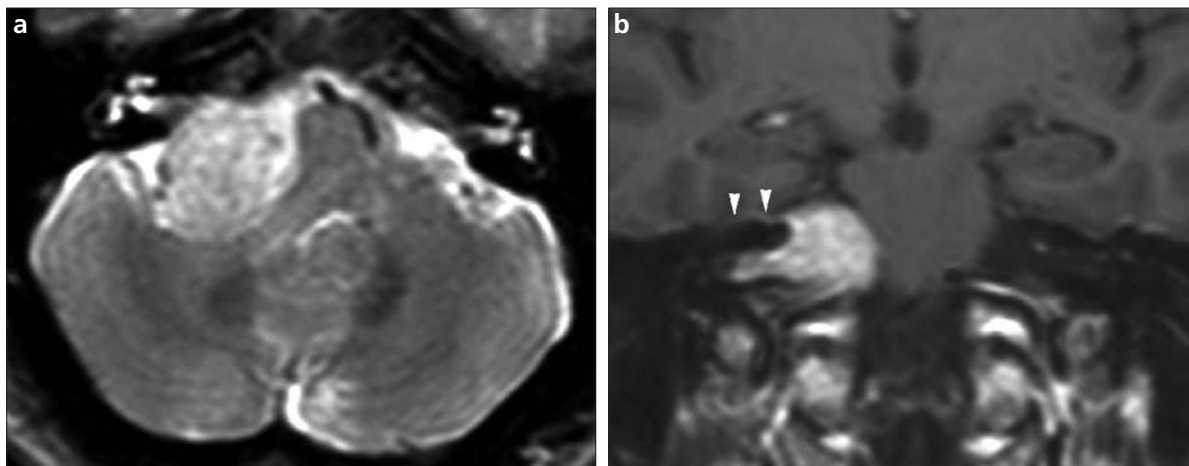
Figure 17. a, b. Meningioma. On transverse T2-weighted **(a)** and contrast enhanced coronal T1-weighted **(b)** MR images, the isointense tumoral lesion compared to gray matter, enhancing homogeneously, shows a dural tail extending along the tentorium *(arrowheads)* and internal acoustic canal. The tentorial extension helps in the differential diagnosis from schwannomas that can otherwise cause a similar view.
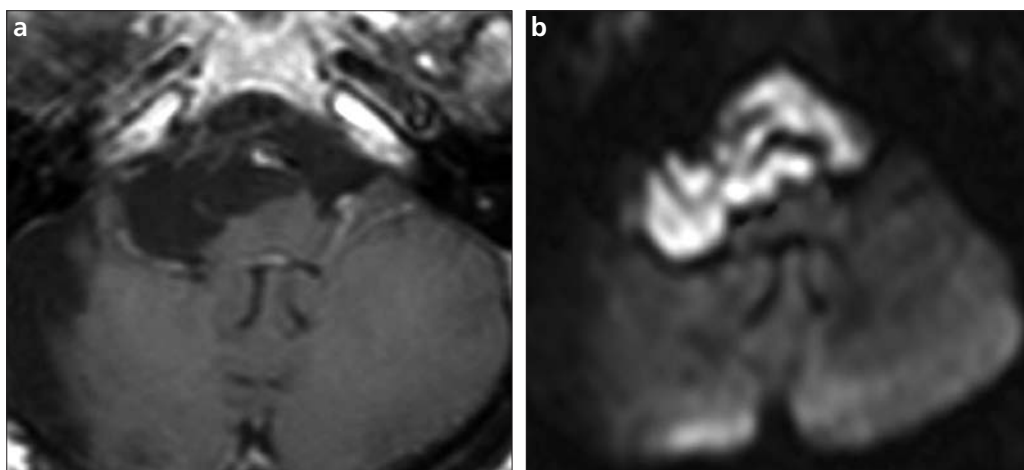
Figure 18. a, b. Epidermoid tumor. On transverse contrast enhanced T1-weighted MR image **(a)**, a cystic lesion, which is isointense compared to cerebrospinal fluid and causing enlargement of the right pontocerebellar angle and prepontine cisterns, does not show prominent enhancement. On transverse diffusion weighted MR image **(b)**, not only the borders of the lesion causing diffusion restriction can clearly be identified, but also its differentiation from the other cystic lesion can be definitely made.

Epidermoid tumors with high keratin content appear hypointense on T1W and hyperintense on T2W images, whereas high cholesterol content results in hyperintensity on T1W images (41). Diffusion restriction is seen on diffusion-weighted MR images (Fig. 18). They are brighter compared to CSF on FLAIR and proton density series (28, 41). These MRI features provide differentiation from other types of tumors, arachnoid cysts, and neurocysticercosis, and make postoperative follow-up easier (28).

MRI is quite effective in the differential diagnosis of tumors occurring in the pontocerebellar angle cistern. In contrast to meningiomas, vestibular schwannomas rarely have a dural tail, and they do not spread above the dorsum sella or into the middle cranial fossa. Occurrence of cerebellar edema is more often in meningiomas. In terms of localization, the predominant part of the tumor is in the internal acoustic canal and the meatus in vestibular schwannomas, whereas meningiomas tend to locate at the middle of the posterior ridge of the petrous bone (meningiomas do not usually enter the internal acoustic canal), and epidermoid tumors are usually located anteriorly or posterolaterally to the brain stem. Vestibular schwannomas cause enlargement, meningiomas cause hyperostosis, and epidermoid tumors cause erosion of the internal acoustic canal. Vestibular schwannomas have a spherical or ovoid shape, whereas meningiomas appear as hemispheres with their base on the dura over the petrous bone, and epidermoid tumors usually have a shape similar to the pontocerebellar angle cistern, or an hourglass shape. Furthermore, the angle that forms between the tumor and the temporal bone is acute and obtuse in schwannomas and meningiomas, respectively. This typical feature of schwannomas results in an ice cream cone appearance (Fig. 16).

The results of nerve-sparing surgery of the internal acoustic canal and pontocerebellar cistern can best be evaluated with thin section 3D T2W gradient echo and contrast enhanced fat suppressed T1W MRI sequences (7, 30). Residue or recurrence of the tumor, and the integrity of the nerve can be evaluated using these methods following nerve-sparing surgery (7) (Fig. 19).

An endolymphatic sac tumor is a papillary cystadenomatous tumor of the
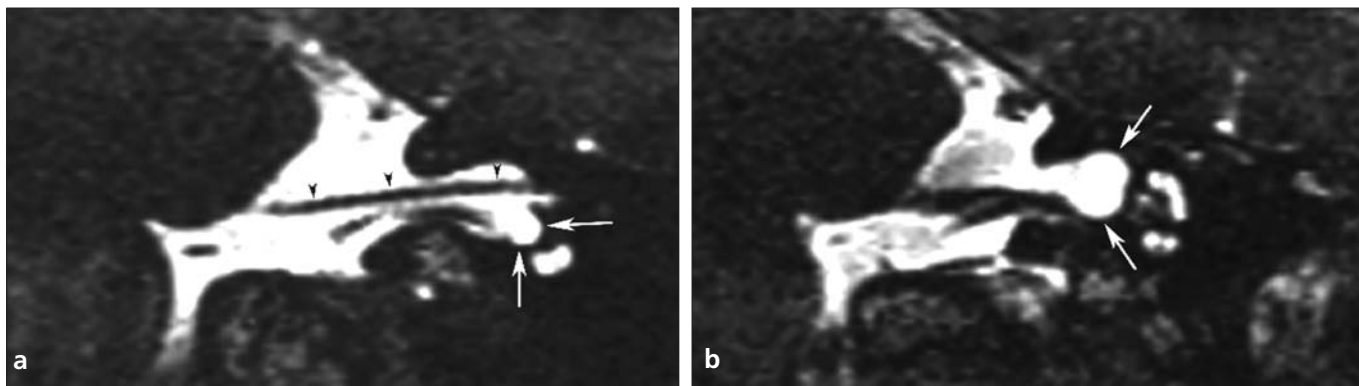
Figure 19. a, b. Postoperative evaluation. On consecutive coronal T2-weighted MR images **(a, b)**, the dilatation of the fundus of the internal acoustic canal *(white arrows)* following tumor resection is shown. The sparing of the facial nerve is postoperatively evident *(a, black arrowheads)*.
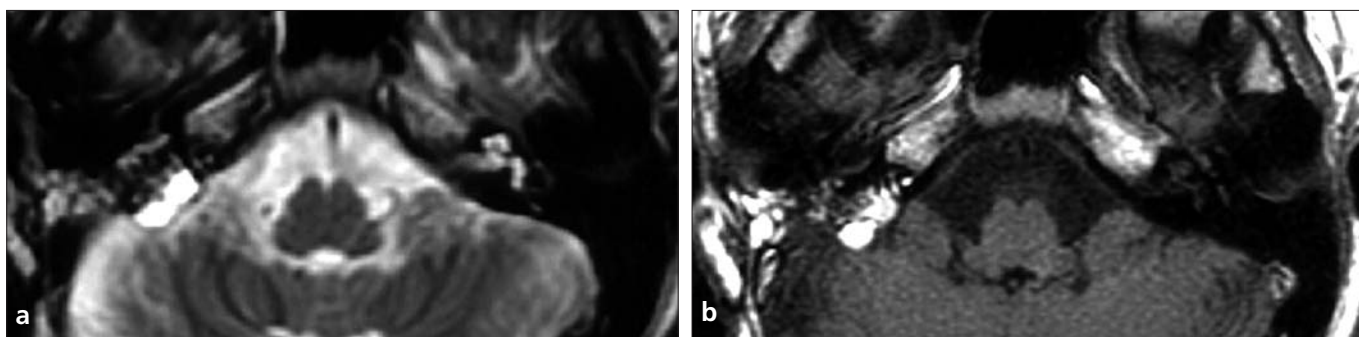
Figure 20. a, b. Endolymphatic sac tumor. On transverse T2-weighted **(a)** and T1-weighted **(b)** MR images, the soft tissue lesion causing dilatation of the right vestibular aqueduct appears hyperintense because of high fat and protein content.
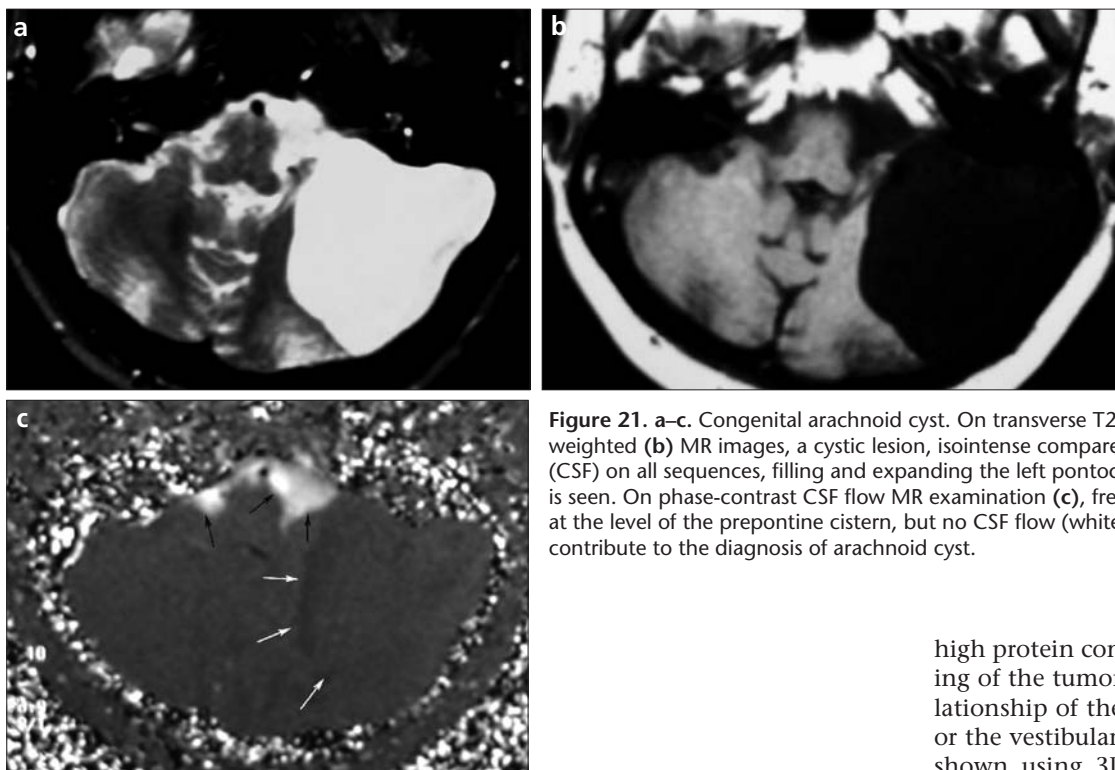
Figure 21. a–c. Congenital arachnoid cyst. On transverse T2-weighted **(a)** and T1-weighted **(b)** MR images, a cystic lesion, isointense compared to cerebrospinal fluid (CSF) on all sequences, filling and expanding the left pontocerebellar angle cistern, is seen. On phase-contrast CSF flow MR examination **(c)**, free CSF flow *(black arrows)* at the level of the prepontine cistern, but no CSF flow (white arrows) in the lesion, contribute to the diagnosis of arachnoid cyst.

temporal bone, usually seen with von Hippel-Lindau disease, and presents with sensorineural hearing loss, abnormal gait, and facial nerve palsy (42). The tumor is heterogeneously hyperintense on T2W images and may appear as hyperintense areas on unenhanced T1W images due to cystic changes with high protein content or internal bleeding of the tumor (42) (Fig. 20). The relationship of the tumor with the SCC, or the vestibular or facial nerve can be shown using 3D gradient echo T2W MRI methods.

A congenital arachnoid cyst is the accumulation of CSF between the split and the double-folded arachnoid membrane, and appears isointense compared to CSF on all MRI sequences
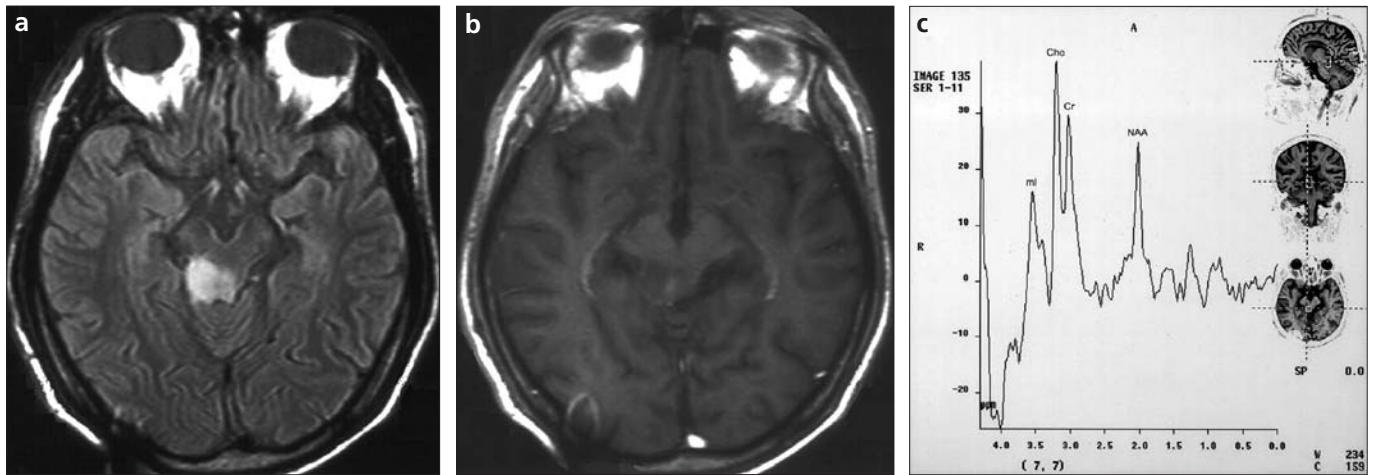
Figure 22. a–c. Tectal glioma. On transverse FLAIR (a) and contrast enhanced T1-weighted (b) MR images, a mass lesion located at the right inferior colliculus is seen. On single voxel MR spectroscopy (TE, 40 ms) (c), a slight reduction in the n-acetyl aspartate/choline ratio and an increase in myo-inositol level indicate a low-grade glial tumor.
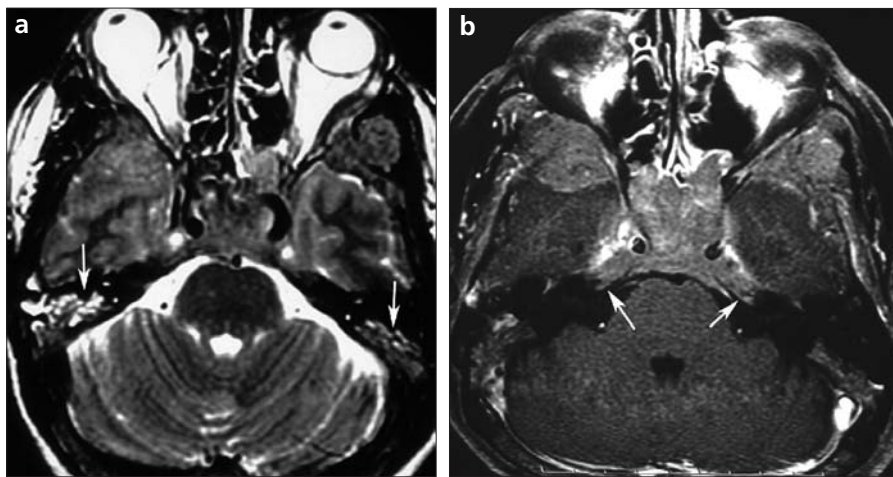
Figure 23. a, b. Petrous apex involvement of nasopharynx cancer. On transverse T2-weighted MR image (a), fluid accumulation *(arrow)* in both middle ear cavities and mastoid cells due to eustachian tube dysfunction is seen. On transverse contrast enhanced fat suppressed T1-weighted MR image (b), the extension of the tumor along both petrous apices *(arrows)* is evident.

(2, 16) (Fig. 21). Hyperintense artifacts within the cyst can be observed due to the internal CSF flow on motion-sensitive sequences like FLAIR. Alterations in the flow of CSF at the level of the pontocerebellar cistern can be shown using phase-contrast MRI methods.

Brain stem gliomas are usually pilocytic (grade I) or diffuse (grade II) astrocytomas. The tumors typically cause enlargement of the brain stem, and compression of the 4th ventricle and pontocerebellar cistern. They appear heterogeneously isointense to hypointense on T1W images and hyperintense on T2W images, and they do not usually enhance, although they sometimes show slight heterogeneous enhancement (Fig. 22). In general, low-grade tumors show increased diffusion, and similar or slightly increased regional cerebral blood volume (rCBV) compared to the cerebellar parenchyma (43, 44). As the grade of the tumor increases, diffusion restriction (decreased ADC values) and increased rCBV values can be seen (43, 44). With MR spectroscopy, the tumors can be separated from the normal brain parenchyma and tumor-like lesions (metastasis, infection, multiple sclerosis, and infarction) because of decreased n-acetyl aspartate levels that become prominent in high-grade tumors, and increased choline and lactate peaks (43).

Tumors that locate in the brain stem, involving the pontocerebellar angle cistern and nerve fibers, include medulloblastoma, cystic cerebellar astrocytoma, and cerebellar hemangioblastoma.

Additionally, ependymoma, choroid plexus papilloma, and carcinomas that arise from the 4th ventricle can extend towards the pontocerebellar angle cistern. Nasopharyngeal, pharyngeal, and parotid carcinomas, multiple myeloma, and tumors of the hypophysis can invade the base of the cranium and spread locally (Fig. 23). Hematogenous metastases may originate from the breast, kidney, and lungs. Bone destruction, associated soft tissue mass, abnormal enhancement, and adjacent tissue involvement are important factors to consider while evaluating metastases (33). Although normal or decreased rCBV values, and an almost normal spectrum with MR spectroscopy of parenchymal metastases and the peritumoral region aid in making the differential diagnosis from primary glial tumors, vague invasion of the adjacent tissues in grade I and II tumors makes this differentiation difficult (43, 44). When located in the pontocerebellar angle cistern, metastases appear as intensely enhancing solid or cystic mass lesions. In general, meningeal involvement in the pontocerebellar angle cistern is typical, and radiological differentiation of these lesions from inflammatory ones is usually impossible. Tumors involving the primary and secondary hearing centers have similar MRI features. Predicting the dominant cerebral hemisphere and the relationship of the tumor to the hearing center using cortical activation studies prior to surgery helps to decrease postoperative morbidity (15).

In conclusion, although CT is the first choice imaging modality for patholo-

gies of the temporal bone, MRI has significant contribution to the diagnosis in the following ways: showing the pathology of the membranous labyrinth; evaluation prior to cochlear implantation; showing complicated infectious and inflammatory diseases; and showing the location and extension of temporal bone tumors. Moreover, MRI must be the first choice when dealing with retrocochlear tumor/infection causing neuro-otologic symptoms, and all kinds of lesions in the brain and brain stem related to the hearing pathways.

References

1. Jäger L, Bonell H, Liebl M, et al. CT of the normal temporal bone: comparison of multi- and single-detector row CT. Radiology 2005; 235:133–141.
2. Casselman JW. Diagnostic imaging in clinical neuro-otology. Current Opinion in Neurology 2002; 15:23–30.
3. Niyazov DM, Andrews JC, Strelioff D, Sinha S, Lufkin R. Diagnosis of endolymphatic hydrops in vivo with magnetic resonance imaging. Otol Neurotol 2001; 22:813–817.
4. Hegarty JL, Patel S, Fischbein N, Jackler RK, Lalwani AK. The value of enhanced magnetic resonance imaging in the evaluation of endocochlear disease. Laryngoscope 2002; 112:8–17.
5. Schick B, Brors D, Koch O, Schafers M, Kahle G. Magnetic resonance imaging in patients with sudden hearing loss, tinnitus and vertigo. Otol Neurotol 2001; 22:808–812.
6. Dobben GD, Raofi B, Mafee MF, Kamel A, Mercurio S. Otogenic intracranial inflammations: role of magnetic resonance imaging. Top Magn Reson Imaging 2000; 11:76–86.
7. Kocaoğlu M, Bulakbaşı N, Üçöz T, et al. Comparison of gadolinium-enhanced T1 weighted and 3D constructive interference in steady state (CISS) sequences in the detection of prognostic factors influencing surgical outcome after hearing-preservation surgery of vestibular schwannomas. Neuroradiology 2003; 45:476–481.
8. Selesnick SH, Rebol J, Heier LA, Wise JB, Gutin PH, Lavyne MH. Internal auditory canal involvement of acoustic neuromas: surgical correlates to magnetic resonance imaging findings. Otol Neurotol 2001; 22:912–916.
9. Pappas DG Jr, Cure JK. Diagnostic imaging. Otolaryngol Clin North Am 2002; 35:1317–1363.
10. Silver RD, Djalilian HR, Levine SC, Rimell FL. High-resolution magnetic resonance imaging of human cochlea. Laryngoscope 2002; 112:1737–1741.
11. Davidson HC. Imaging evaluation of sensorineural hearing loss. Semin Ultrasound CT MR 2001; 22:229–249.
12. Counter SA, Bjelke B, Borg E, Klason T, Chen Z, Duan ML. Magnetic resonance imaging of the membranous labyrinth during in vivo gadolinium (Gd-DTPA-BMA) uptake in the normal and lesioned cochlea. Neuroreport 2000; 11:3979–3983.
13. Naidich TP, Mann SS, Som PM. Imaging of the osseous, membranous, and perilymphatic labyrinths. Neuroimaging Clin N Am 2000; 10:23–34.
14. Phelps PD. Fast spin echo MRI in otology. J Laryngol Otol 1994; 108:383–394.
15. Yetkin FZ, Roland PS, Mendelsohn DB, Purdy PD. Functional magnetic resonance imaging of activation in subcortical auditory pathway. Laryngoscope 2004; 114:96–101.
16. Mark AS, Casselman JW. Anatomy and diseases of the temporal bone. In: Atlas SW, ed. Magnetic resonance imaging of the brain and spine, Vol. 2. Philadelphia: Lippincott Williams & Wilkins, 2002; 1363–1432.
17. Valvassori GE, Buckingham RA. Imaging of temporal bone. In: Valvassori GE, Mafee MF, Carter BL, eds. Imaging of head and neck. New York: Thieme Medical Publishers, 1995; 1–156.
18. Wilson-Pauwels L, Akesson EJ, Stewart PA. Cranial nerves, anatomy and clinical comments. Toronto: BC Decker, 1988; 98–113.
19. Rubinstein D, Sandberg EJ, Cakade-Law AG. Anatomy of the facial and vestibulocochlear nerves in the internal auditory canal. AJNR Am J Neuroradiol 1996; 17:1099–1105.
20. Greenstein B, Greenstein A. Color atlas of neuroscience. Neuroanatomy and neurophysiology. Stuttgart, New York: Thieme. 2000; 254–271.
21. Tan EK, Chan LL. Clinico-radiologic correlation in unilateral and bilateral hemifacial spasm. J Neurol Sci 2004; 222:59–64.
22. Schaefer PW, Ozsunar Y, He J, et al. Assessing tissue viability with MR diffusion and perfusion imaging. AJNR Am J Neuroradiol 2003; 24:436–443.
23. de Sousa LC, Piza MR, da Costa SS. Diagnosis of Meniere's disease: routine and extended tests. Otolaryngol Clin North Am. 2002; 35:547–564.
24. Marsot-Dupuch K, Meyer B. Cochlear implant assessment: imaging issues. Eur J Radiol 2001; 40: 119–132.
25. Cochlear Implants in Adults and Children. NIH Consensus Conference. J Am Med Assoc 1995; 274:1955–1961.
26. Demirpolat G, Savas R, Totan S, Bilgen I, Kirazli T, Alper H. Temporal bone CT and MRI in cochlear implant candidates. Tani Girisim Radyol 2003; 9:41–46.
27. Kebapçı M, Adapınar B, Özkan R, Kaya M. Sensorinöral işitme kayıplarında geniş vestibüler kanal: YRBT bulguları. Türk Radyoloji Dergisi 1998; 33:598–601.
28. Stasolla A, Magliulo G, Lo Mele L, Prossomariti G, Luppi G, Marini M. Value of echo-planar diffusion-weighted MRI in the detection of secondary and postoperative relapsing/residual cholesteatoma. Radiol Med (Torino) 2004; 107:556–568.
29. Chang P, Fagan PA, Atlas MD, Roche J. Imaging destructive lesions of the petrous apex. Laryngoscope 1998; 108:599–604.
30. Williams MT, Ayache D. Imaging of the postoperative middle ear. Eur J Radiol 2004; 14:482–495.
31. Heimert TL, Lin DDM, Yousem DM. Case 48: Osteogenesis imperfecta of the temporal bone. Radiology 2002; 224:166–170.
32. Bergamaschi R, Romani A, Zappoli F, Versino M, Cosi V. MRI and brainstem auditory evoked potential evidence of eighth cranial nerve involvement in multiple sclerosis. Neurology 1997; 48:270–272.
33. Dolan KD. Malignant lesions of the ear. Radiol Clin North Am 1974; 12:585–600.
34. Appling D, Jenkins HA, Patton GA. Eosinophilic granuloma in the temporal bone and skull. Otolaryngol Head Neck Surg 1983; 91:358–365.
35. Brackmann DE, Owens RM, Friedman RA, et al. Prognostic factors for hearing preservation in vestibular schwannoma surgery. Am J Otol 2000; 21:417–424.
36. Somers T, Casselman J, de Ceulaer G, Govaerts P, Offeciers E. Prognostic value of magnetic resonance imaging findings in hearing preservation surgery for vestibular schwannoma. Otol Neurotol 2001; 22:87–94.
37. Hampton SM, Adler J, Atlas MD. Evaluating the role of magnetic resonance imaging scans in the surgical management of acoustic neuromas. Laryngoscope 2000; 110:1194–1197.
38. Moriyama T, Fukushima T, Asaoka K, Roche PH, Barrs DM, McElveen JT Jr. Hearing preservation in acoustic neuroma surgery: importance of adhesion between the cochlear nerve and the tumor. J Neurosurg 2002; 97:337–340.
39. Lapsiwala SB, Pyle GM, Kaemmerle AW, Sasse FJ, Badie B. Correlation between auditory function and internal auditory canal pressure in patients with vestibular schwannomas. J Neurosurg 2002; 96:872–876.
40. Maiuri F, Iaconetta G, de Divitiis O, Cirillo S, Di Salle F, De Caro ML. Intracranial meningiomas: correlations between MR imaging and histology. Eur J Radiol 1999; 31:69–75.
41. Robert Y, Carcasset S, Rocourt N, Hennequin C, Dubrulle F, Lemaitre L. Congenital cholesteatoma of the temporal bone: MR findings and comparison with CT. AJNR Am J Neuroradiol 1995; 16:755–761.
42. Bulakbaşı N, Örs F, Uğurel Ş, Taşar M, Somuncu İ. Von Hippel Lindau sendromunda izlenen kraniospinal tutulumun radyolojik değerlendirilmesi. Tani Girisim Radyol 2001; 7:439–445.
43. Bulakbasi N, Kocaoglu M, Ors F, Tayfun C, Ucoz T. Combination of single voxel proton MR spectroscopy and apparent diffusion coefficients calculation in the evaluation of common brain tumors. AJNR Am J Neuroradiology 2003; 24:225–233.
44. Cha S. Update on brain tumor imaging: from anatomy to physiology. AJNR Am J Neuroradiol 2006; 27:475–487.